# Combined High Spectral Resolution Lidar and Millimeter Wavelength Radar Measurement of Ice Crystal Precipitation

DOE Grant DE-SC0006933 Final Report

Dr. Edwin Eloranta, Principal Investigator
University of Wisconsin – Madison
1225 West Dayton Street
Madison, WI 53706

For the period of: 15-Sept-2011 to 14-Sept-2015

10/28/2016

#### Abstract

The goal of this research has been to improve measurements of snowfall using a combination of millimeter-wavelength radar and High Spectral Resolution Lidar (HSRL) Observations. Snowflakes are large compared to the 532nm HSRL wavelength and small compared to the 3.2 and 8.6 mm wavelength radars used in this study. This places the particles in the optical scattering regime of the HSRL, where extinction cross-section is proportional to the projected area of the particles, and in the Rayleigh regime for the radar, where the backscatter cross-section is proportional to the mass-squared of the particles. Forming a ratio of the radar measured cross-section to the HSRL measured cross section eliminates any dependence on the number of scattering particles, yielding a quantity proportional to the average mass-squared of the snowflakes over the average area of the flakes. Using simultaneous radar measurements of particle fall velocities, which are dependent particle mass and cross-sectional area it is possible to derive the average mass of the snow flakes, and with the radar measured fall velocities compute the snowfall rate.

Since this retrieval requires the optical extinction cross-section we began by considering errors this quantity. The HSRL is particularly good at measuring the backscatter cross-section. In previous studies of snowfall in the high Arctic were able to estimate the extinction cross-section directly as a fixed ratio to the backscatter cross-section. Measurements acquired in the STORMVEX experiment in Colorado showed that this approach was not valid in mid-latitude snowfalls and that direct measurement of the extinction cross-section is required. Attempts to measure the extinction directly uncovered shortcomings in thermal regulation and mechanical stability of the newly deployed DOE HSRL systems. These problems were largely mitigated by modifications installed in both of the DOE systems. We also investigated other sources of error in the HSRL direct measurement of extinction (see appendix II of this report). We also developed improved algorithms to extract extinction from the HSRL data. These have been installed in the standard HSRL data processing software and are now available to all users of HSRL data.

Validation of snowfall measurements has proven difficult due to the unreliability of conventional snowfall measurements coupled with the complexity of considering the vast variety of snowflake geometries. It was difficult to tell how well the algorithm's approach to accommodating differences in snowflakes was working without good measurements for comparison. As a result, we decided to apply this approach to the somewhat simpler, but scientifically important, problem of drizzle measurement. Here the particle shape is known and the conventional measurement are more reliable. These algorithms where successfully applied to drizzle data acquired during the ARM MAGIC study of marine stratus clouds between California and Hawaii (see Appendix I). This technique is likely to become a powerful tool for studying lifetime of the climatically important marine stratus clouds.

## **Detailed Project Report**

Due to maintenance issues at the North Slope ARM site, combined HSRL/radar snowfall data was not available during the first year of this project. Research focused on testing the underlying algorithms using data acquired from Steamboat Springs, Colorado during the DOE STORMVEX project.

Our retrieval algorithms use a combination of lidar extinction, radar backscatter cross sections and radar fall velocities to measure snowfall rates without needing to assume an ice crystal shape. The lidar extinction cross section is directly related to the average area of the snow-flakes. While the radar backscatter cross section is directly related to the average mass-squared of the flakes and the fall velocity is related to both cross-sectional area and mass of the flakes. In previous retrievals of snowfall rates (derived from a long-term deployment at Eureka weather station on Ellesmere Island, Nunavut) we assumed that the extinction coefficient could be determined from the backscatter cross section scaled by an average value of the backscatter phase function. The assumed backscatter phase function of 0.038 1/sr was derived from a long term cirrus cloud data set and it provided a good representation of the monthly accumulation of snowfall at Eureka. It also provided useful but less exact comparisons with the daily gauge measurements. Attempts to use direct HSRL measurements of the extinction cross section did not seem to improve the retrieval accuracy. This was attributed to extinction measurements errors caused by instabilities in the overlap correction of this first generation remotely controlled HSRL. It is also likely that the cold temperatures of this high Arctic site yield ice crystals that are similar to those found in cirrus clouds, thus making the cirrus derived phase function a good fit.

Under the support of this grant we examined this approximation in more detail. STORMVEX data from Steamboat Springs, Colorado has been used to look at fluctuations in the backscatter phase function in mid-latitude snowfall. Direct extinction measurements with the HSRL face two challenges. First, unlike the backscatter cross section, the extinction measurement is not derived from a ratio of two channels where the geometric correction of near range signals cancel. Secondly, the extinction cross section is derived from the range derivative of the molecular backscatter signal and derivatives are intrinsically noisy. Snowfall also rapidly attenuates the lidar signal, decreasing the number of photons counted and increasing statistical noise in the signal. The snowfall rates in Colorado are much larger than in Eureka, making this a bigger problem in STORMVEX data.

The angular field-of-view used in the DOE HSRL systems have been increased from the 40 micro radians used in the Eureka system to 100 micro radians in order increase the stability of this geometric correction. However, initial data from the this lidar showed geometric instabilities caused by changing temperature gradients within the instrument. It was necessary to install additional Peltier temperature control units to minimize these gradients. This was not sufficient to stabilize near range extinction measurements. A prolonged investigation identified an additional cause of alignment drift. Humidity changes appear to warp the edge of the lidar optical bench. This is apparently related to moisture absorption in adhesives that bond the stainless steel surfaces to the internal honeycomb core. The alignment stability of the AMF HSRL was greatly improved by moving the support point for two mirrors away from the edge of the optical bench. This improved near range extinction measurements but did not completely eliminate the problem. A study of errors in the extinction measurement presented in appendix II illustrates the issues. We began our work by systematically using the routine calibration sequences automatically acquired during STORMVEX to update calibrations for the entire experiment

period. Careful examination of the molecular backscatter signals demonstrated the difficulty in maintaining sufficient temporal and spatial resolution to depict the rapidly varying snowfall features while still achieving sufficient averaging to suppress noise in the retrieved extinction. A major upgrade of extinction algorithms in the HSRL software was undertaken. This implements Savitsky-Golay filters in both the range and time dimensions. It employs a sliding polynomial fit that allows more aggressive filtering with less distortion of the signal. This has been added to routine HSRL data processing software with adjustable averaging parameters that allow a user to balance the competing requirements for resolution and accuracy as needed. These improvements allow successful recovery of the apparent extinction cross section in snowfall. We have also investigated the use of a constrained fitting algorithms for the time-range variation of the retrieved molecular scattering. Constraints are provided by the known monotonic decrease of the retrieved molecular signal with range, the known Possion distribution of photon counting noise and the knowledge that the extinction is highly correlated with the more robustly measured backscatter cross section. This helped to motivate an independently funded investigation of extinction retrieval algorithms reported in "A new Approach to Inverting Backscatter and Scatter from Photon-Limited Lidar Observations", W. J. Marris, R. E. Holz, Y. H. Hu, R. E. Kuehn, E. W. Eloranta and R. M. Willet, Accepted for publication in Applied Optics.

We then turned our attention to backscatter phase function variations in snowfall. Figures 1-4 show the limitations of assuming a constant backscatter phase function. Figures 1 and 2 show the extinction cross section and the depolarization measured in a STORMVEX snow shower observed on 26-Jan-2011. Water clouds, seen as horizontal layers with high extinction and low deodorization, exist at altitudes of ~5 km and ~4 km. Parts of the prominent snow shower seen between 5:30 and 6:30 UT show high depolarization as expected from non-spherical ice crystals. However, the leading edge of the shower (~5:30 to ~5:45UT) shows depolarization much lower than are expected for irregular ice crystals. This suggests the presence of specular reflections from the faces of ice crystal plates. Because the lidar is pointed at 4 degrees off of zenith to avoid specular reflection from horizontally oriented plates, these plates must be tumbling or oscillating in order to direct the reflections back to the lidar. Figure 3 shows that these specular reflections dramatically increase the backscatter cross section in the low depolarization streamer while the extinction image is rather smoothly varying in the shower. As a result, the backscatter phase function plotted in figure 4 also shows dramatic variations--suggesting that assuming a constant value for the backscatter phase function in snowfall algorithms is likely to produce large errors. The relatively good agreement found using this assumption with the Eureka data may be due to colder conditions that produce different crystal types at Eureka and partly due to comparisons that averaged over many separate snow showers with different crystal types.

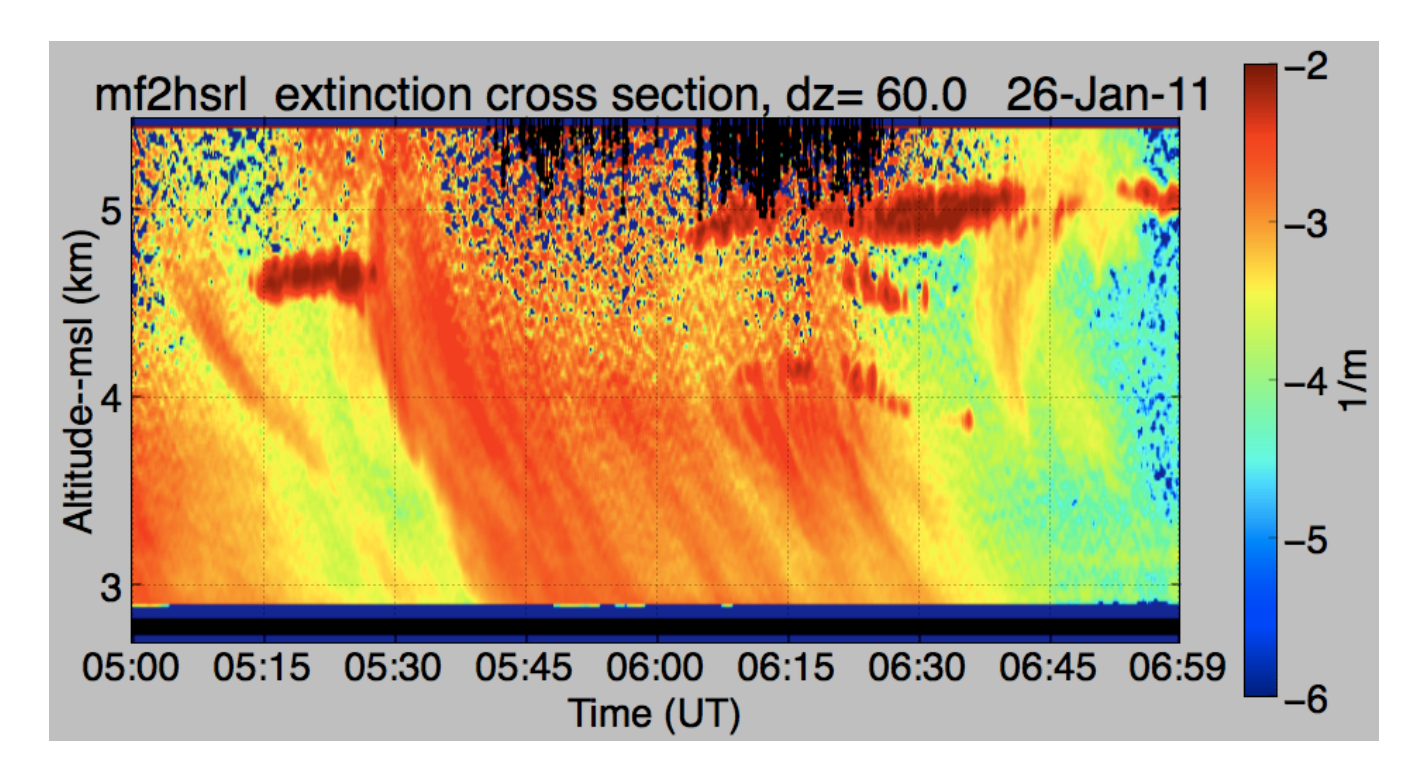


Figure 1. Extinction cross section in a STORMVEX snow shower. The extinction cross section is computed from the derivative of the molecular backscatter profile measured by the HSRL and is directly proportional to the projected area of ice crystals.

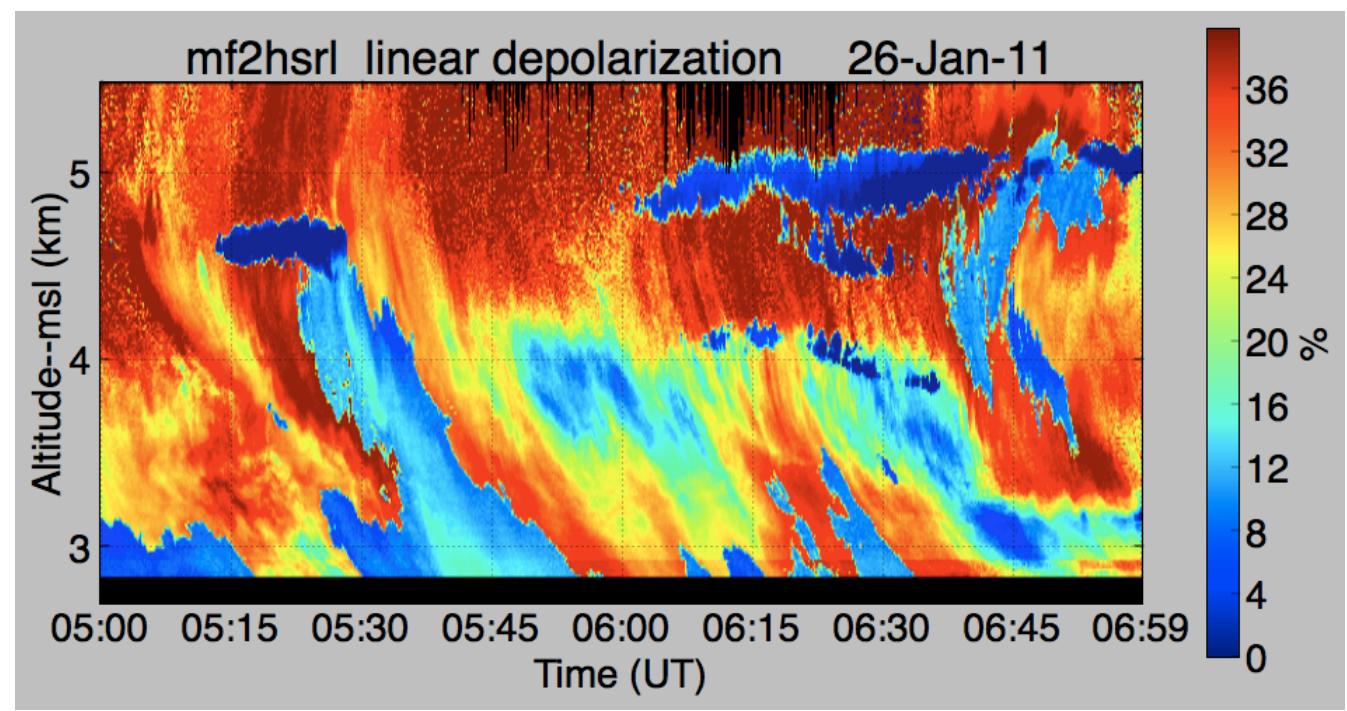


Figure 3: Depolarization image from a STORMVEX snow shower. High depolarization results when light is scattered from non-spherical particles while low depolarization occurs when light is scattered from spherical particles or when the scattering is dominated by specular reflection from a plane surfaces.

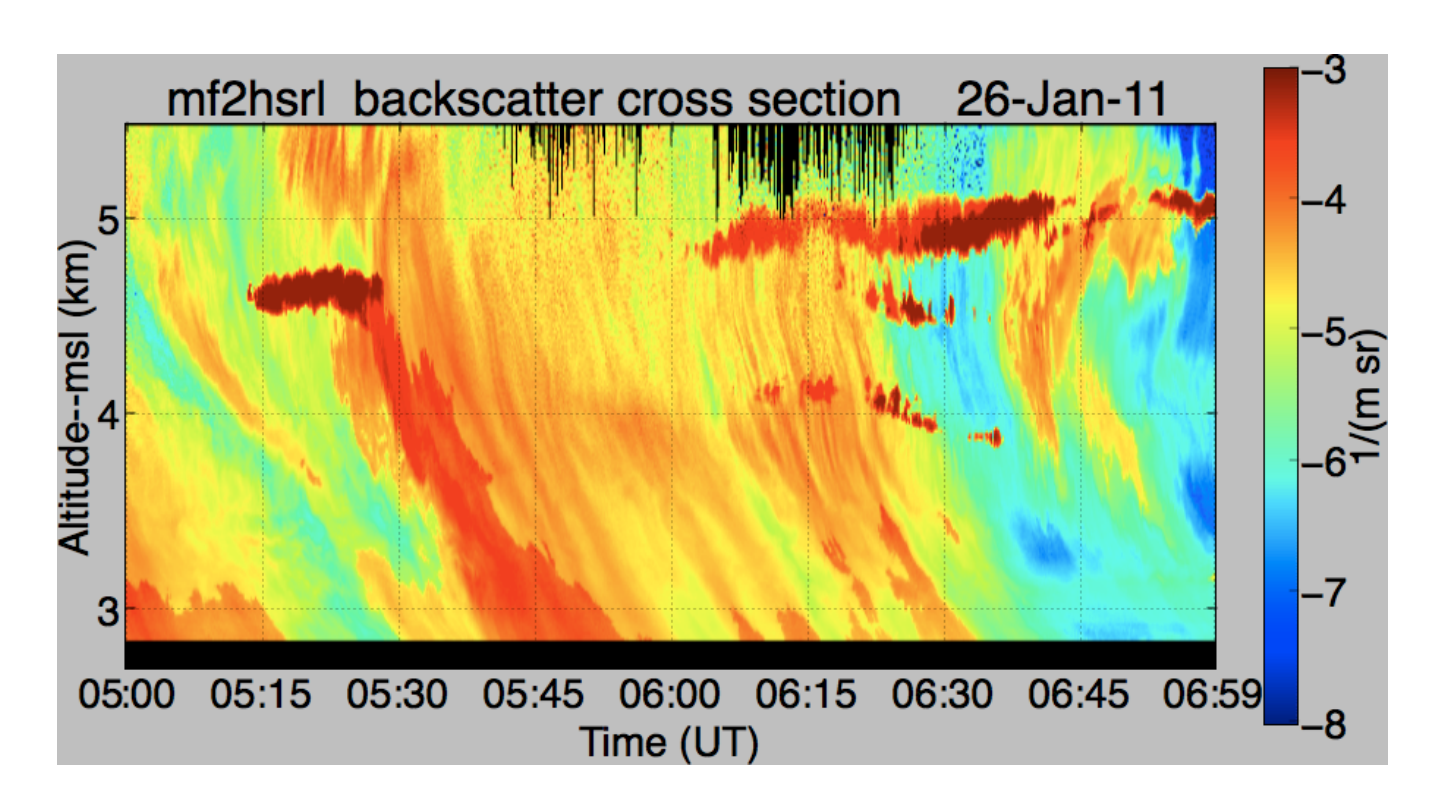


Figure 3: Backscatter cross section image in a STORMVEX snow shower.

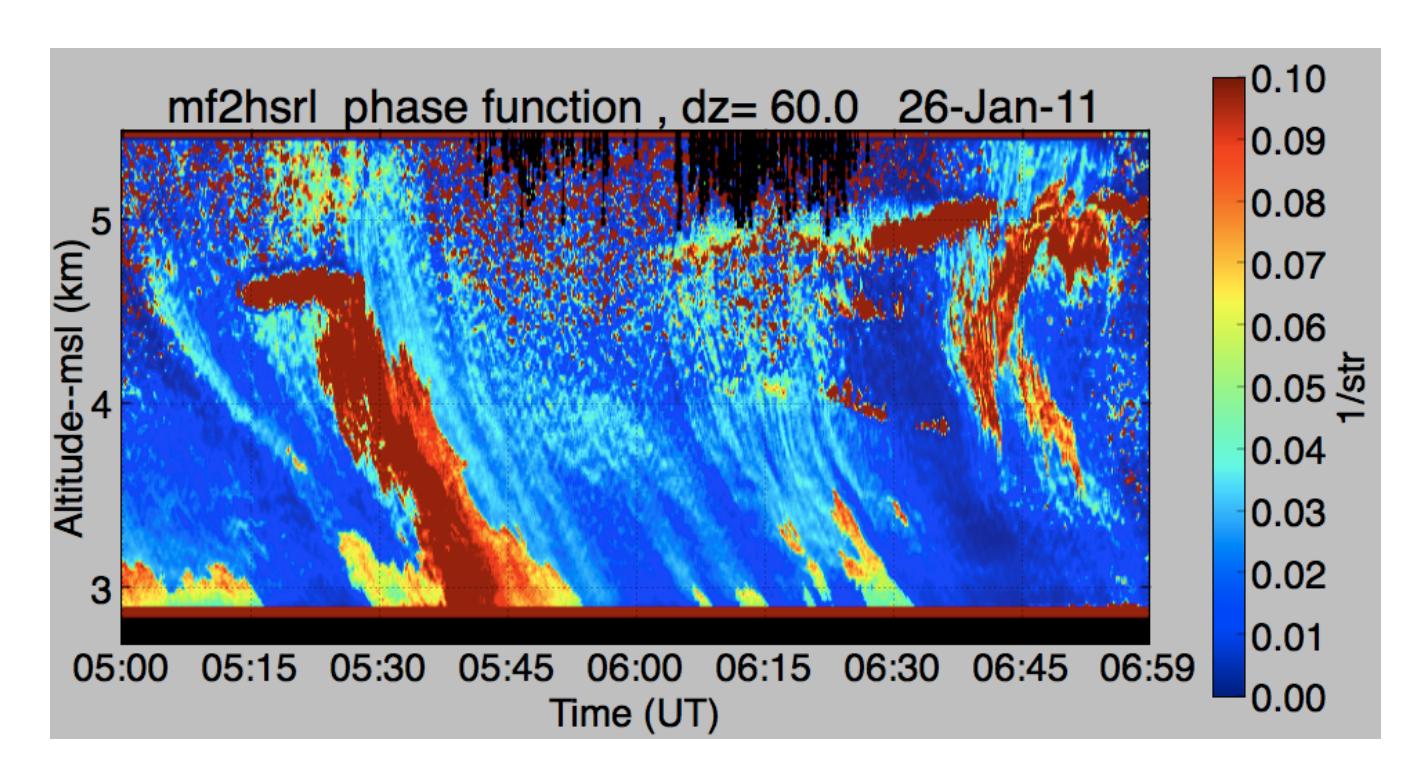


Figure 4: Backscatter phase function in a STORMVEX snow shower. The backscatter phase function is the ratio between the backscatter cross section and the extinction cross section. The dramatic variations within the snow shower shows that snowfall retrievals should be based on direct measurement of the extinction cross section rather

than attempting to derive the extinction from backscatter cross section measurements using an assumed backscatter phase function.

Collaboration with other ARM researchers has resulted in submission of a paper "Arctic Multi-Layered, Mixed-Phase Cloud Processes Revealed in Doppler Spectra " authored by Johannes Verlinde, Mahlon P. Rambukkange, Eugene E. Clothiaux, Greg M. McFarquhar, and Edwin W. Eloranta. This investigation indicates the frequent presence of drizzle along with ice crystals in precipitation from arctic mixed-phase clouds. This rather unexpected result is likely to explain some of the HSRL observed depolarization and backscatter phase function variations we observed during STORMVEX. It also has important ramifications in modeling the life cycle of mixed-phase clouds, since both drizzle formation and ice nucleation must be accurately represented in order to estimate the rate of water removal from the cloud layer.

Evaluation of ice crystal precipitation retrievals is hampered by the lack of reliable conventional snowfall measurements, the great variability of snow crystal morphology and sensitivity of Doppler fall velocities to vertical air motion. In particular, conventional snowfall measurements are so unreliable that they provide little help in testing the accuracy of the retrievals. This made it difficult to separate the effects of measurement error from algorithm assumptions. Applying the basic radar-lidar precipitation measurement technique to the somewhat simpler problem of drizzle measurement offers a parallel problem without unknown particle shapes, somewhat lower sensitivity to air motion, and better conventional measurements. In addition, robust drizzle measurements are important in addressing critical issues regarding the maintenance of marine stratus clouds. Considerable progress was achieved in applying the lidar-radar retrievals to drizzle data acquired during the DOE MAGIC campaign. This work is described in Appendix I.

# APPENDIX I

Presented at the International Laser Radar Conference, ILRC27

New York, New York

5-10 July, 2015

# DRIZZLE MEASUREMENTS USING HIGH SPECTRAL RESOLUTION LIDAR AND RADAR DATA

Edwin W. Eloranta

University of Wisconsin, Madison, WI 53706, USA, \*Email: eloranta@ssec.wisc.edu

#### **ABSTRACT**

The ratio of millimeter radar and High Spectral Resolution Lidar (HSRL) backscatter are used to determine drizzle rates which are compared to conventional ground based measurements. The robustly calibrated HSRL backscatter cross section provides advantages over measurements made with traditional lidars.

#### 1. INTRODUCTION

Marine stratus clouds are an important feature of the global climate system. Cloud lifetime is sensitive to drizzle rates. Drizzle not only removes water from the cloud but evaporation of the falling droplets cools the sub-cloud layer acting to suppress convection. Accurate measurements of drizzle rates will improve our understanding of cloud maintenance.

Several investigators have used simultaneous lidar and radar observations to determine particle size However, measurements made [1.2.3]. conventional lidar are hampered by: 1) changes in the transmission of the output window caused by water accumulation, 2) the difficulty of correcting the backscatter signal for atmospheric extinction, 3) the effects of multiple scattering, and 4) the need to convert backscatter measurements to extinction. The use of High Spectral Resolution Lidar(HSRL) data avoids many of these problems. backscatter measurements are referenced to the known molecular scattering cross-section at each point in the profile and are thus independent of changes in window and atmospheric transmission.

This study uses data collected during the US Department of Energy Atmospheric Sciences program MAGIC campaign. Instruments including a suite of conventional precipitation gauges, a High Spectral Resolution Lidar, along with 3.2 mm wavelength WACR and a 8.6 mm wavelength KAZR radars, were installed on the container ship *Horizon Spirit* as it made repeated trips between Long Beach, CA and Honolulu, HI. Figures 1 though 4 provide an example of the measurements used in our retrieval of drizzle rates.

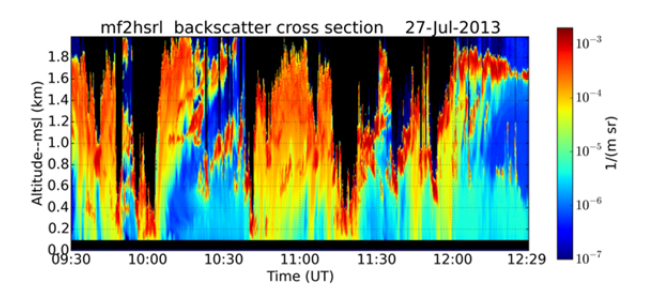


Figure 1: HSRL measured 532nm backscatter cross-section on 27-Jul-2013. Water clouds produce the areas with backscatter cross-sections near 1e-3 1/(m sr). Drizzle shafts near the surface appear with backscatter cross-sections between 1e-5 and 1e-4 1/(m sr).

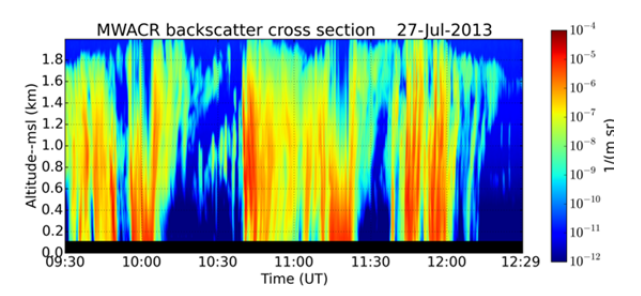


Figure 2: Radar backscatter cross section measured with the WACR 3.2 mm wavelength radar. (note: cross section is 4  $\pi$  times usual radar definition).

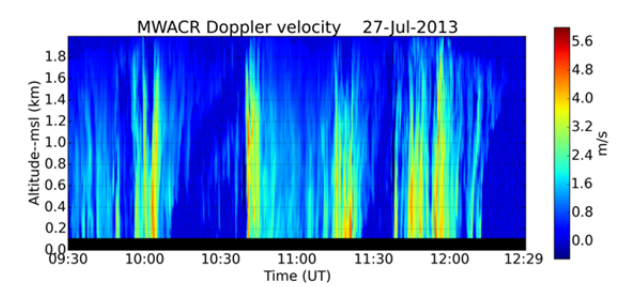


Figure 3: Doppler velocity measured with the WCAR radar on 27-Jul-2013.

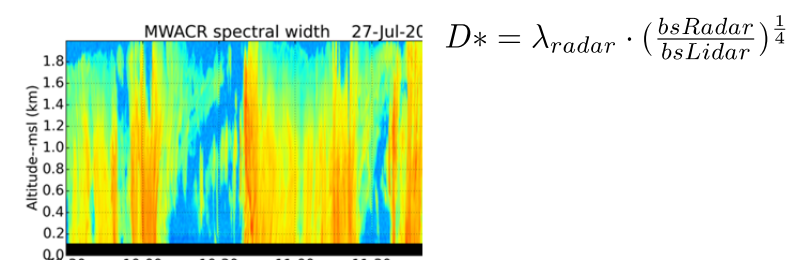


Figure 4: Spectral width measured with the WACR radar on 27-Jul-2013.

#### 2. DIZZLE PARTICLE SIZE RETRIEVAL

We assume a modified gamma distribution [4] of particle diameters:

$$\frac{dN}{dD} \sim D^{\alpha} \cdot exp(-\frac{\alpha}{\gamma} \cdot (\frac{D}{D_m})^{\gamma})$$

Where: N = number of particles

D = particle diameter

 $D_m = mode diameter$ 

 $\alpha, \gamma$  = shape parameters

Using Mie theory we compute the backscsatter cross-section as a function of size parameter for both 532nm and 8.6 mm wavelengths using the appropriate indices of refraction. Calculations extend over the range of diameters between 1 micron and 5 mm. The optical cross-sections were carried out at size parameter intervals of 0.01 and averaged to a spacing of 1 size parameter.

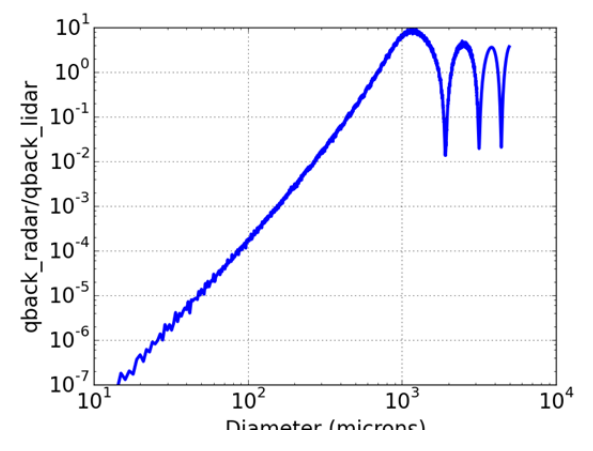


Figure 5: Ratio of radar ( $\lambda$ =3.2 mm) to lidar ( $\lambda$ =532 nm) backscatter efficiencies for monodisperse particle size distribution.

It is convenient to define a diameter D\* as a ratio of the radar and lidar backscatter cross-sections:

This ratio can be computed for our size distribution using Mie theory backscatter efficiencies  $Q_{bsRadar}$  for radar and  $Q_{bsLidar}$  for lidar scattering along with the radar wavelength,  $\lambda_{radar}$ :

$$D* = \lambda_{radar} \cdot \left(\frac{\int D^2 \cdot N(D) \cdot Q_{bsRadar} \cdot dD}{\int D^2 \cdot N(D) \cdot Q_{bsLidar} \cdot dD}\right)^{\frac{1}{4}}$$

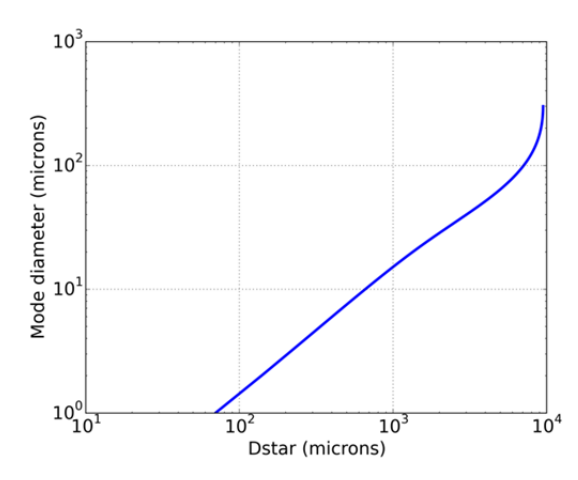


Figure 6: The relationship between D\* and mode diameter for a modified gamma distribution calculated with  $\gamma$ =0.7 and  $\alpha$ =1 for lidar and radar wavelengths of 532nm and 3.2 mm respectively at a temperature of 285K.

This relationship allows mode diameters to be derived from D\* measurements. Formulating the relationship in terms of the backscatter cross-section takes advantage of the robustly calibrated HSRL measurement. This measurement does not require corrections for window transmission or atmospheric extinction below the scattering volume. In addition, multiple scattering effects largely cancel out in the HSRL backscatter retrieval.

Using Mie theory for the radar avoids errors caused by the Rayleigh approximation. However, the maximum mode diameter which can be retrieved is limited because the relationship between D\* and the mode diameter becomes multi-valued when the particle sizes increase into the Mie regime .

Because the size distribution is known the mode diameter can be easily converted to effective diameter (effective diameter = ratio of particle volume to area).

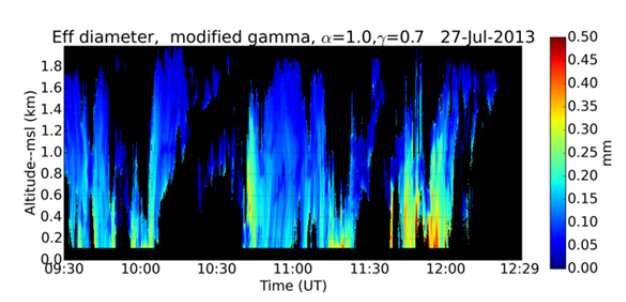


Figure 7: Effective diameter for the data shown with  $\xi$ =1  $\square$   $\square$   $\gamma$ =0.7.

Beard's parameterization [5] of fall velocity is used to compute the radar cross-section weighted fall velocity. The radar measured Doppler velocity and spectral width are independent measurements that can be compared to the modeled radar weighted velocities. Values of the shape parameters,  $\alpha$  and  $\gamma$  can be adjusted to improve the comparison between the measured and modeled velocities.

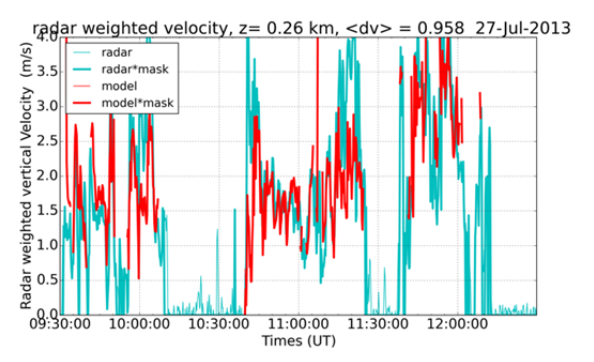


Figure 8: Comparison between measured Doppler velocities and the modeled radar weighted fall velocity at an altitude of 130 m with  $\alpha = 1$ ,  $\gamma = 0.7$ .

Even though we do not expect exact agreement because the Doppler velocity includes contributions due to vertical air motion, figures 8 and 9 show good agreement between the retrieved radar weighted velocities and the measured Doppler velocities.

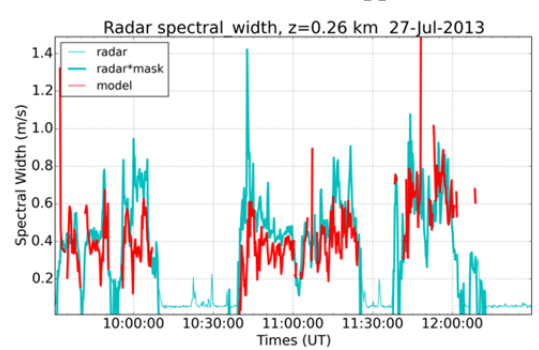


Figure 9: Comparison of measured and modeled spectral width as a function of time at an altitude of 130 m assuming  $\alpha = 1 \square \square \square \gamma = 0.7$ .

#### 3. DRIZZLE RATE RETRIEVAL

The extinction cross-section, of particles that are large compared to the wavelength is twice the geometric area [6]:

$$\beta_{ext} = 2 \cdot N < A >$$

Where:

N = particle number density

<A> = average geometric area of particles

Because the effective diameter is  $<D^3>/<D^2>$ , the liquid water content(LWC) can be computed using the density of water:

The lidar extinction cross-section is derived from the lidar backscatter cross-section using:

#### Where:

 $Q_{ext}$  and  $Q_{bs}$  are extinction and backscatter efficiencies calculated from Mie theory.

$$LWC = \frac{1}{3} \cdot \rho_w \cdot D_{eff} \cdot \beta_{ext}$$

$$\beta_{ext} = bsLidar \cdot \frac{\int D^2 \cdot N(D) \cdot Q_{ext}(D) \cdot dD}{\int D^2 \cdot N(D) \cdot Q_{bs}(D) \cdot dD}$$

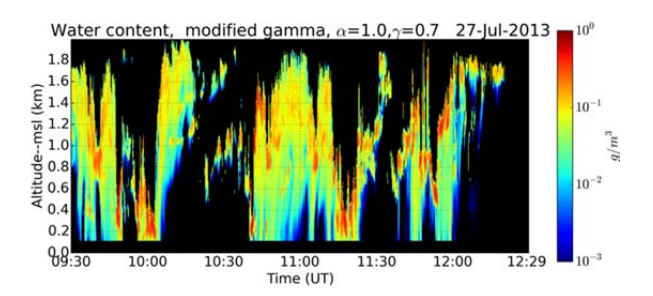


Figure 10: Liquid water content.

The derived liquid water content is not valid where clouds and drizzle are present together because this retrieval has assumed a mono-modal size distribution.

With the particles size distribution known, the mass weighted fall velocity can be computed using the Beard parameterization. The precipitation rate is computed from the product of the mass weighted fall velocity and the liquid water content.

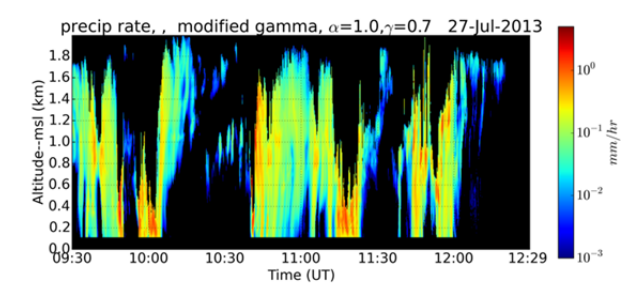


Figure 11: Precipitation rate image for 27-Jul-2013 derived using  $\alpha = 1$ ,  $\gamma = 0.7$ .

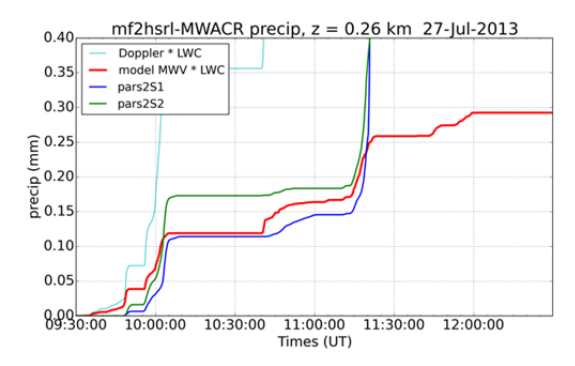


Figure 12: The accumulated precipitation measured by two shipboard distrometers (pars2S1 and pars2S2) and the lidar-radar retrieval. Also shown is the derived liquid water content multiplied by the radar Doppler velocity.

Figure 11 highlights the difficulty of making conventional precipitation measurements on a moving ship. Lidar-radar retrievals agree with PAR2S1 measurements prior to 11:45 UT, but do not agree as well with PARS2S2 measurements. After 11:45UT, the two distrometers give very different precipitation rates. Two conventional rain gauges on the ship also provide wildly different precipitation rates. Using the 8.6mm KAZR radar data in the retrieval indicated ~10% less precipitation with a best fit to velocities using  $\gamma$  ~ 0.5. This difference may be related to radar calibrations differences or because the WACR antenna was gyro-stabilized, while KZAR pointing angle rolled with the ship.

#### 4. CONCLUIONS

Lidar-Radar drizzle retrievals using HSRL data show considerable promise. The technique is sensitive to the functional form of the assumed size distribution and needs to be tested in a setting where more accurate conventional measurements are possible.

#### **ACKNOWLEDGEMENT**

This research was support by Department of Energy Grant DE-SC0006933.

#### REFERENCES

- [1] Interi J.M., J. L. Stephens, W. L. Eberhard and, T. Uttal, 1993: A Method for Determining Cirrus Cloud Particle Sizes Using Lidar and Radar Backscatter Technique, *J. Applied Meteor.*, **32**, 1074-1082.
- [2] Donovan, D.P., and A.C.A.P. van Lammeren, 2001: Cloud effective particle size and water content profile retrievals using combined lidar and radar observations: 1. Theory and examples, *J. Geophy. Res. Atmos.*, **106**, 27425-27448.
- [3] O'Connor, E. J., A. J. Illingworth, R. J. Hogan, 2004: Retrieving Statocumulus Drizzle Parameters Using Doppler Radar and Lidar, *J. Atmos. Ocean Tech.*, 21(5), 777-778.
- [4] Deirmendjain, D., 1969: *Electromagnetic Scattering on Spherical Polydispersions*. American Elsevier, 290 pp.
- [5] Beard, K. V., 1976: Terminal velocity and shape of cloud and precipitation drops aloft. *J. Atmos. Sci.*, **33**, 851–864.
- [6] van de Hulst, H. C., 1957: *Light Scattering by Small Particles*. John Wiley and Sons, 470 pp.

# Appendix II

# Presented at IEEE Aerospace Conference

1 - 8 March, 2014

Big Sky, Montana

# High Spectral Resolution Lidar Measurements of Atmospheric Extinction: Progress and Challenges

Edwin Eloranta

University of Wisconsin-Madison
Space Science and Engineering Center
1225 W. Dayton St
Madison, WI 53706
608-262-7327

eloranta@ssec.wisc.edu

Abstract—High Spectral Resolution lidar (HSRL) systems have proven capable of providing nearly continuous calibrated profiling of atmospheric backscatter cross-section and depolarization. These are combined to provide detailed images of aerosol and cloud structure. They also provide calibrated measurements of atmospheric extinction. Atmospheric values of the 1/e extinction length range from less than 100 m in water clouds to greater than 100 km in clear weather. While backscatter cross-section and depolarization are derived from ratios of HSRL signals that cancel out range sensitive

instrumental artifacts, extinction measurements are derived from the molecular backscatter return alone. Furthermore, extinction is derived from the slope of the molecular signal. This amplifies noise due to photon counting statistics. Signal strengths vary over nearly 6-decades within the ~20 km useful clear air range of the lidar or within a few hundred meters in a dense water cloud. These factors make extinction measurements more demanding than the backscatter cross-section measurements and often preclude useful measurements in conditions of interest.

### **TABLE OF CONTENTS**

| 1. Introduction                   | 2 |
|-----------------------------------|---|
| 2. OVERLAP FUNCTION ERRORS        | 4 |
| 3. THE TEMPERATURE PROFILE ERRORS |   |
| 4. Photon Counting Errors         |   |
| 5. ACTUAL EXTINCTION MEASUREMENTS |   |
| 6. SUMMARY                        |   |
| References                        |   |
| BIOGRAPHY                         |   |

# 1. Introduction

The University of Wisconsin has designed and constructed a family of five High Spectral Resolution Lidars designed for untended operation in remote locales. One of these is installed in the National Center for Atmospheric Research Gulfstream 5 aircraft, while others have been deployed in the high Arctic, Singapore, the Maldives, a Colorado ski

mountain, and on a container ship making regular voyages between California and Hawaii. These systems have proven capable of providing nearly continuous calibrated profiles of atmospheric backscatter cross-section and depolarization that yield exquisite, calibrated images of aerosol and cloud structure. High Spectral Resolution Lidar (HSRL) systems [1, 2] transmit light with a bandwidth of less than 100 MHz. When this light is backscattering from atmospheric molecules it is Doppler broadened to approximately 3 GHz by the thermal motion of the molecules. In contrast, backscattering from atmospheric particulate matter returns with nearly the same spectral width as the transmitted light. This spectral difference is used to separate the lidar signal into independent molecular,  $S_{\rm m}$ , and particulate,  $S_{\rm p}$ , profiles.

$$\begin{split} S_p(r) &\sim t_w \cdot \eta(r) \cdot \frac{1}{r^2} \cdot \frac{P(180,r)}{4\pi} \cdot \beta_p(r) \cdot e^{-2\int_0^r \beta_e(r)dr} \text{(1)} \\ S_m(r) &\sim t_w \cdot \eta(r) \cdot \frac{1}{r^2} \cdot \frac{3}{8\pi} \cdot \beta_m(r) \cdot e^{-2\int_0^r \beta_e(r)dr} \text{ (2)} \end{split}$$

#### Where:

t<sub>w</sub> = Shelter window transmission

 $\boldsymbol{\eta} = \text{Overlap}$  between laser beam and receiver field of view

r = Range from lidar

 $\beta_m$  = Molecular scattering cross-section (1/m)

 $\beta_p$  = Particulate scattering cross-section (1/m)

P(180, r) = backscatter phase function (1/sr)

 $\beta_e$  = Extinction cross-section (1/m)

An equation for the particulate backscatter cross-section is obtained from the ratio between the particulate and molecular equations. Notice that the window transmission, the overlap factor and the atmospheric extinction terms all cancel out allowing calculation of the particulate backscatter cross-section as the product of the scattering cross-section and the backscatter phase function.

$$\frac{P(180,r)}{4\pi} \cdot \beta_p(r) = \frac{3}{8\pi} \beta_m(r) \cdot \frac{S_p(r)}{S_m(r)} \tag{3}$$

Because the molecular scattering cross-section,  $\beta_m$ , is directly proportional to the molecular density it can be calculated from an independently provided temperature sounding.

The advantage of the HSRL is seen by comparing the attenuated backscatter cross-section measured with a normal aerosol backscatter lidar shown in Figure 1 with the HSRL measurement of calibrated backscatter cross-section shown in Figure 2.

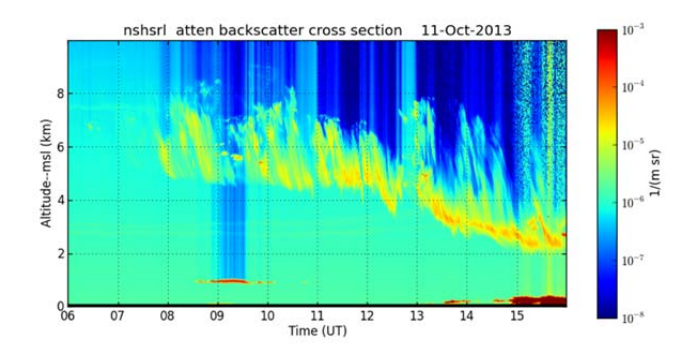


Figure 1: Attenuated total backscatter cross-section observed with the HSRL combined channel output treated as a standard aerosol backscatter lidar on 11-Oct-2013 in Barrow, Alaska.

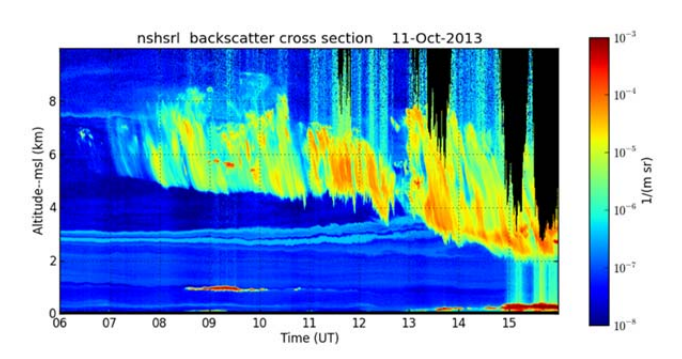


Figure 2: HSRL calibrated particulate backscatter crosssection derived for the case shown in Figure 1.

The HSRL measurement completely removes the attenuation artifacts evident behind the low cloud at 9:00 UT and in the upper part of the cirrus cloud seen above 2 km in Figure 1. In addition, the tenuous aerosol layers at approximately 3 km become clearly visible in the HSRL result because the molecular scattering has been removed. Standard lidar systems are also poorly suited for measurements in rain or snow because the shelter window transmission varies as precipitation accumulates on the window. In contrast, decreased window transmission lowers the HSRL signal to noise ratio but does not affect the calibration.

The HSRL provides robust measurements of the backscatter cross-section; the extinction cross-section is a more desirable measurement. The extinction cross-section determines how much sunlight penetrates though the atmosphere and it plays a central role in determining visibility through the atmosphere. Also, in the case where particles are significantly larger than the laser wavelength, the extinction cross-section is directly proportional to the projected area of the particle. Most atmospheric clouds have little absorption at visible wavelengths. In this case, the scattering cross-section is equal to the extinction cross-

section. Yet, it still difficult to use the backscatter crosssection to estimate extinction because the backscatter phase function is sensitive to the particle size distribution, the index of refraction, and shape. It varies over an order of magnitude from approximately 0.01 to 0.12.

The atmospheric extinction cross-section can be derived by taking the log of the equation for  $S_m(r)$  and then differentiating with respect to range:

$$\beta_e(r) = \frac{1}{2} \cdot \frac{d}{dr} [log(\frac{\eta(r) \cdot \beta_m(r)}{r^2 \cdot S_m(r)})] \tag{4}$$

This provides the total extinction cross-section as function of the measured molecular signal and the molecular scattering cross-section computed from an independently provided sounding. The extinction due to particulates alone can be derived by simply subtracting the molecular extinction cross-section.

The remainder of this paper will look at the errors involved when measuring the extinction cross-section directly using this equation.

# 2. Overlap Function Errors

Because the extinction cross-section is computed from only the molecular signal and not a ratio of two signals, the overlap function,  $\eta(r)$ , is part of Equation 3. The overlap function corrects for that fraction of the backscattered light that arrives at the field stop of the receiving telescope but fails to pass through the stop. Part of the light may be blocked because the image spot is not centered on the stop or because it is out of focus. The University of Wisconsin HSRL design uses a single telescope for both the transmitter and the receiver such that the transmit beam and the receiver field of view are coaxial. As a result the image spot is always centered on the field stop. However, the receiving telescope is focused on infinity and thus, the image of the scattering volume is poorly focused in the near range. Figure 3 shows the overlap function for one of the Wisconsin HSRL systems. Full overlap,  $\eta = 1$ , is reached when the image spot becomes smaller than the field stop. In the Wisconsin HSRL systems this occurs between 4 and 6 km. At close ranges the correction becomes very large.

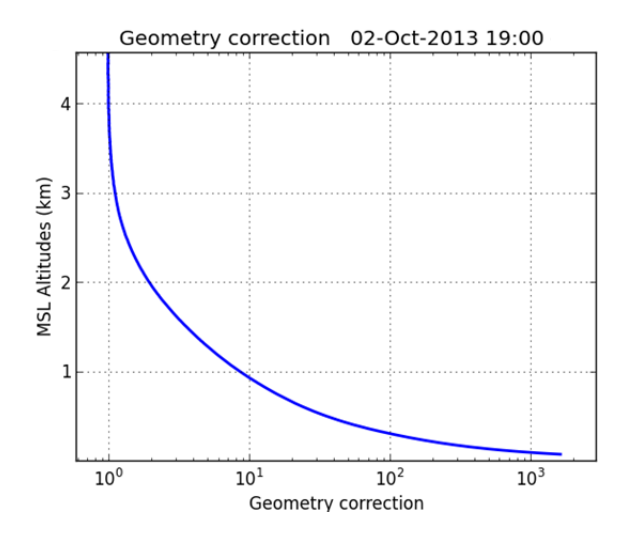


Figure 3. Overlap correction,  $\eta(r)$ , for one of the University of Wisconsin's HSRL systems.

While it is possible to make full overlap occur closer to the lidar, by increasing the field stop diameter, this would introduce too much background noise. Eye safety limits the maximum energy density in our transmitted beam. This requires the system operate at high repetition rate (4 kHz) with small energies in each pulse. Scattered sunlight adds noise to the signal recorded for each pulse: this makes it necessary to operate with a small receiver angular field-ofview. Operation at eye safe wavelengths in either the infrared or ultraviolet could overcome the eye safety problem. Infrared operation is not practical because the inverse fourth-power dependence of Rayleigh scattering makes the molecular signal very weak. Operation in the UV is possible. However, our 532nm wavelength is desirable because: 1) it is at the peak of the solar spectrum and thus important to studies of energy flow in the atmosphere, 2) it is at the peak sensitivity of our eyes and is thus appropriate for visibility measurements, and 3) it allows us to use an iodine absorption line as a blocking filter to separate particulate and molecular signals [1].

In practice, the above equation is used to derive the extinction cross-section. Applying the overlap and r-squared corrections before taking the log reduces the dynamic range creating easier-to-filter signals. Although not used in this form, it is instructive to write the equation

as follows: 
$$\beta_e(r) = \frac{1}{2\eta} \frac{d\eta}{dr} + \frac{1}{2\beta_m} \frac{d\beta_m}{dr} - \frac{1}{r} + \frac{1}{S_m} \frac{dS_m}{dr}$$
 (5)

We begin examining the overlap term and its influence on measurement of boundary layer aerosols. The molecular extinction cross-sections in the boundary layer is  $^{\sim} 10^{-5} \, \text{m}^{-1}$ . Aerosol extinction on clear days is often less than the molecular. Thus, it would desirable to measure extinction cross-section values less than  $10^{-6} \, \text{m}^{-1}$ . Figure 4 plots the

first term on the right-hand side of this equation for one of the University of Wisconsin HSRL's.

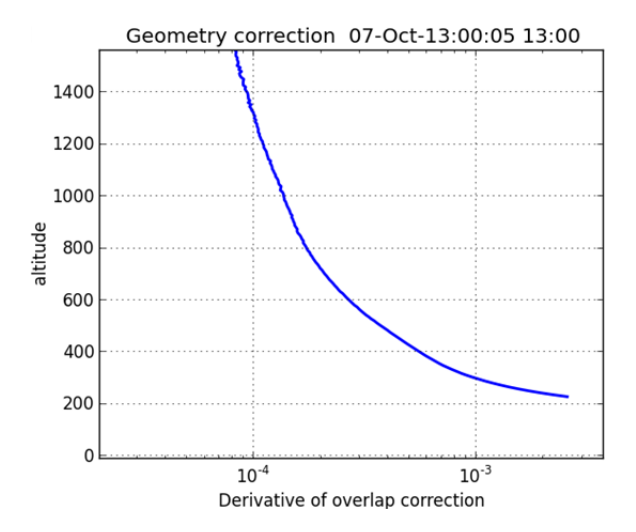


Figure 4. Log-derivative overlap correction – the first term on the right-hand side of Equation 5.

At an altitude of 300 m this term has a value of  $10^{-3}$  m<sup>-1</sup>. Thus, to measure the extinction cross-section at this altitude with an uncertainty of  $10^{-6}$  m<sup>-1</sup>, the overlap correction must be known to 0.1%. Unfortunately, very small changes in system alignment or in the energy distribution within the transmitted laser beam produce large changes in the near range overlap correction. The UW HSRL design works to minimize this sensitivity by using very stable optical mounts contained in a temperature controlled housing. A single 20-times beam expanding telescope is used for the transmitter and receiver to ease alignment of the receiver with the transmit beam.

The overlap correction,  $\eta(r)$ , must be measured after each optical alignment or any change in the laser operating conditions. This measurement can be made by rearranging Equation 2 to provide  $\eta(r)$  as a function of  $S_m(r)$  and  $\beta_m(r)$ and assuming that  $\beta_e$  is due only to molecular scattering.  $S_m(r)$  is measured on a very clear day while  $\beta_m(r)$  is computed from an independently measured sounding. This simple measurement has one major drawback—the boundary layer almost always contains some aerosol and the aerosol attenuation introduces uncertainty into the correction. Relatively clear days suitable for this calibration have been found during operations at Madison Wisconsin, and in the Arctic at Eureka, Nunavut and Barrow, Alaska. On the other hand, during one-year of operation in Singapore, a persistent dense boundary aerosol layer made this calibration nearly impossible. The error due to residual aerosol attenuation can be reduced by independently measuring the optical depth of the atmosphere and then assuming that the scattering phase function of the aerosol is independent of altitude. The backscatter cross-section derived from Equation 3 can then be used to distribute the extinction cross section in altitude. The aerosol extinction can be corrected for in the computation of  $\eta(r)$ . For the Singapore operations we have used a sun photometer to measure the optical depth of the entire atmosphere at the laser wavelength and for the Wisconsin and Arctic measurements where the aerosol optical depth is already small we use an assumed value of the backscatter phase function and Equation 3 to approximate the aerosol extinction.

Even with the sun photometer measurements it has been difficult to make good measurements of  $\eta(r)$  in Singapore where scattered boundary layer clouds are nearly always present.

In our most recent HSRL system we have included a wide field-of-view (wfov) channel to improve characterization of  $\eta(r)$ . This channel uses a 2.5-cm diameter telescope mounted behind the secondary mirror of the main telescope. It is coupled via optical fiber to a second molecular HSRL channel consisting of a interference filter, an etalon to block sky background light, and a molecular iodine filter to block aerosol scattering. This channel duplicates the molecular of the HSRL except that it views a 1 mr angular field-of-view rather that the 0.1 mr viewed by the main molecular channel. The wfov channel provides complete overlap, with  $\eta(r)$  equal to 1, at only 375 m from the lidar. But, since it views a solid angle 100 times as large as the main channel using an objective with 0.0039 times the area, it suffers from poor noise performance. Figure 5 shows a comparison of signals from the two molecular channels.

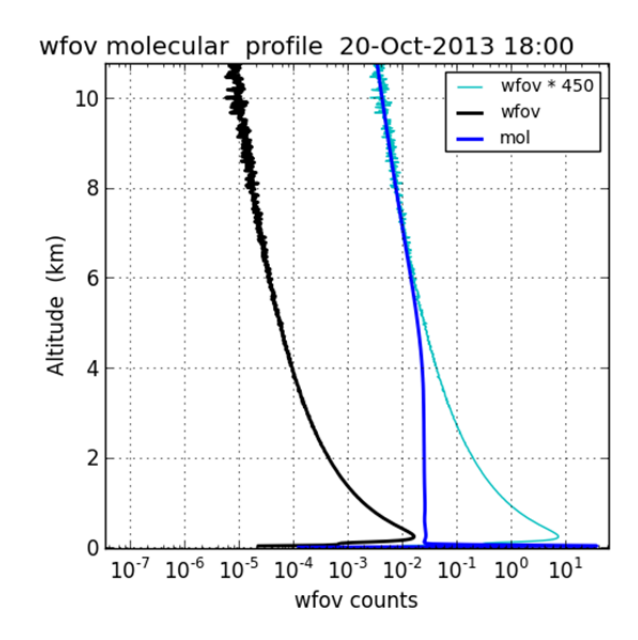


Figure 5: A comparison of the molecular wide field-ofview channel signal (black) and the standard narrow fieldof-view molecular channel (blue). Also shown is the wfov view signal rescaled to match the narrow channel at

higher altitudes (cyan). These measurements were made in Huntsville, Alabama.

A comparison of the narrow and rescaled wide field-of-view channels (Figure 5) shows that complete overlap does not occur until  $^{\sim}$  6 km in this system. Above 6 km  $\eta(r)$  is assumed equal to one. Below 6 km and above  $^{\sim}400$  m  $\eta(r)$  is obtained from the ratio of the signals in the wide and narrow field-of-view channels (Figure 6). Generation of the correction factor below 400 m relies on cases with a well-mixed boundary that extends above 400 m where we can measure both the extinction and the backscatter cross-section accurately. Equation 3 is used to derive the backscatter phase function and this value is assumed to hold below 400 m so that it is possible to estimate the extinction from the backscatter cross-section.

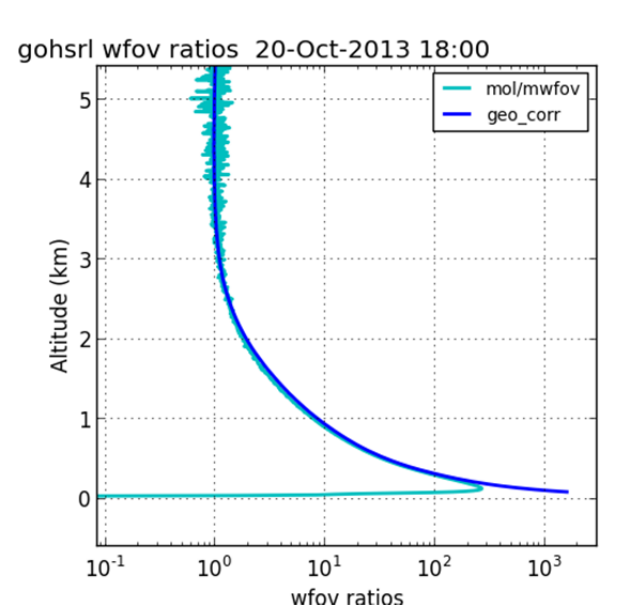


Figure 6: The ratio between the rescaled wfov and the standard molecular channel signals (cyan). Also shown is  $\eta(r)$  after the correction is extended by estimating extinction below 400 m from the measured backscatter phase function in that part of the mixed layer above 400 m. These measurements were made in Huntsville, Alabama.

# 3. The Temperature Profile Errors

The second term on the right-hand side of Equation 5 is evaluated from an independently measured temperature profile. The molecular extinction cross-section is directly proportional to the atmospheric density so that for a vertically pointing lidar:

$$\frac{1}{\beta_m} \frac{d\beta_m}{dz} = \frac{1}{\rho} \frac{d\rho}{dz} = -\frac{1}{T} \left( \frac{dT}{dz} - \frac{g}{R} \right) \tag{6}$$

Where:  $\rho$  = density, g = acceleration of gravity, z = altitude, and R = gas constant.

The temperature resolution to achieve a given  $\beta_e$  error can be obtained by differentiating Equation 6 with respect to temperature.

$$\Delta \beta_e = \frac{1}{T^2} \cdot \left(\frac{dT}{dz} + \frac{g}{R}\right) \cdot \Delta T$$
 (7)

Thus, at a temperature of 300 K and a lapse rate, dT/dz = 6 K/km a temperature error ~2 K produces a ~10<sup>-6</sup> m<sup>-1</sup> error in extinction cross-section. It takes more than a 20 K temperature error to produce a  $10^{-5}$  m<sup>-1</sup> extinction error. Thus, it becomes possible to use twice daily temperature sounding for all but the most sensitive extinction measurements.

# 4. Photon Counting Errors

We now consider the final term of Equation 5. Errors in the logarithmic range derivate of the molecular signal are dependent on how accurately the HSRL calibration separates molecular and particulate signals as well as statistical photon counting errors. In most cases, photon counting errors dominate. The molecular signal,  $S_{\rm m}$ , is derived from the number photons detected in the HSRL molecular,  $N_{\rm m}$ , and combined,  $N_{\rm c}$ , channels of the instrument:

$$S_m(r) = k(r) \cdot (N_m(r) - C_{am}N_c(r))$$
(8)

Outside of clouds  $N_m$  and  $N_c$  are of similar magnitude, while  $C_{am} < 0.0005$  and thus the combined channel contribution can be neglected outside of clouds. The last term of Equation 5 can then be written as:

$$\frac{1}{S_m(r)} \frac{dS_m}{dr} = \frac{1}{k(r)} \frac{dk(r)}{dr} + \frac{1}{N_m(r)} \frac{d(N_m(r) + N_b)}{dr}$$
 (9)

Notice that the range derivative now also includes the background counts from sky and detector noise,  $N_b$ . Although the average number of background counts does not vary with range, counting errors will appear as range variations.

The first term on the right hand side includes the range variation of the calibration coefficients used to separate molecular and particulate photons. These coefficients are determined through calibration of the spectral bandpass of the receiver channels and knowledge of the atmospheric temperature profile. They are quite well measured and almost always dominated by photon counting error contributions to the  $N_{\rm m}$  term.

Photon counting errors are explained via Poisson statistics where the signal variance is equal to the number of photon counts. The problem posed by the  $N_{\rm m}$  term can be seen by approximating the error for best case where the molecular photon counting rate is near the point of detector saturation. The Geiger-mode avalanche photodiode detectors used in our HSRL systems are unable to count

more than 1 photon per 7.5 m range bin. With the system operating at a 4 kHz repetition rate and a 2.5 second averaging time, a single range bin can count a maximum of  $10^4$  photons in one sample. Approximating the derivative from the counting error for 2.5-second profiles and a separation of one range bin shows that photon counting statistics provide a large source of error.

m<sup>-1</sup> (10)

Even in this case with very strong signals, the error is approximately three orders of magnitude larger than the  $10^{-6} \, \text{m}^{-1}$  extinction cross-section we might like to measure. Clearly, it will be necessary to average over longer time and space intervals to reduce errors anywhere near those that are desired.

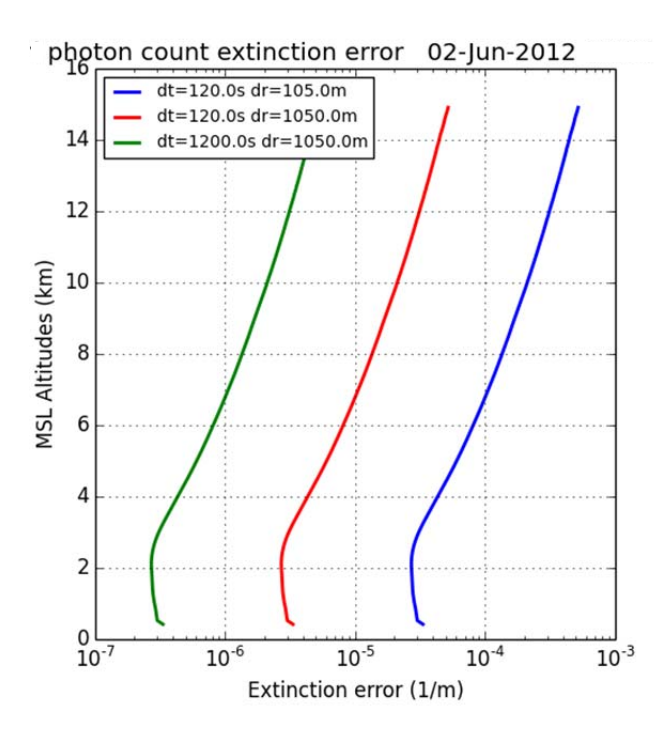


Figure 7: Extinction errors due to photon counting statistics for different time and range averages estimated from the last term on the left-hand side of Equation 8. These results computed from clear-air returns on 2-June-2012.

Figure 7 shows that photon counting errors in the extinction measurement can be reduced below 10<sup>-6</sup> m<sup>-1</sup> below 7 km using 20 minute time and 1 km range averaging. However, this amount of averaging will not be practical in most cases because it will obscure the temporal and spatial scales of the atmospheric structures present.

# 5. Actual Extinction Measurements

The backscatter cross-section image in Figure 8 shows typical atmospheric variability. The dense water cloud just

below 2 km has a depth of less than 200 m and many small cloud elements pass through the lidar observed volume in less than ten minutes. It is clear that the data would be badly degraded if the data were averaged into 20 minute time and 1 km altitude blocks to suppress photon counting noise.

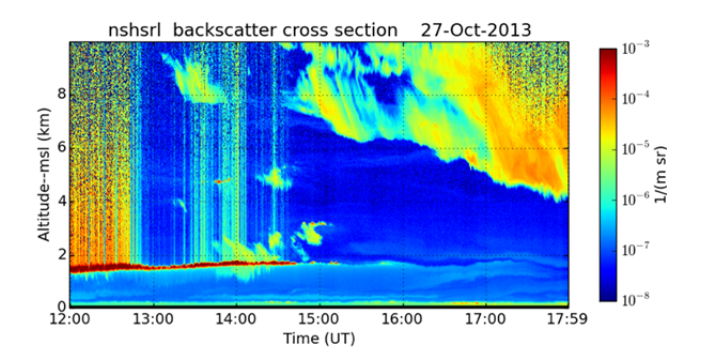


Figure 8. Example of HSRL backscatter cross-section data illustrating the spatial and temporal scales present in the atmosphere. Measurements were made in Barrow, Alaska.

In order to preserve the spatial structure while still decreasing the photon counting statistical fluctuations, extinction cross-sections are derived using Savitzky-Golay filtering [3]. Savitzky-Golay filtering is widely used in spectroscopy to filter spectra while maintaining the shape of spectral lines. In our computation of extinction, a polynomial is first fit to the log term in Equation 4. The fit is applied to a moving time window at each altitude. Each data point is replaced with the mid-point value of the polynomial centered at that point. A second polynomial is then fit to the time filtered data in a moving altitude window at each time. The derivative in Equation 4 is derived from the derivative of the polynomial at the center point and the extinction is derived from Equation 4.

Figure 9 shows the extinction cross-section derived using 60 second time and 30 m altitude averaging. The extinction was not calculated for data with a molecular channel signal-to-noise ratio less than 5. A time window of 360 seconds and an altitude widow of 300 m where used with 3<sup>rd</sup> order Savitzky-Golay filtering. The averaging and window lengths were selected starting from small values and increasing them until errors other than photon statistical fluctuations limit the minimum extinction. In Figure 9 these errors can be seen as horizontal feature extending through the entire time period. They are caused by errors in the overlap function. Errors appear as horizontal structures, because the same overlap function is applied to all profiles. These features appear at a level of ~3x10<sup>-5</sup> m<sup>-1</sup> and they provide the noise floor. The current instruments and algorithms provide useful measurement for particulate extinction values greater than ~10<sup>-4</sup> m<sup>-1</sup>.

We hope to improve on this limit. A decreased noise floor can be achieved by increasing the transmitted laser power. Eye safe operation can be maintained by flattening the Gaussian distribution of energy in the transmitted beam, allowing nearly twice as much average power without exceeding eye safe limits. Errors in the overlap function are due to photon noise in the measurement and derivative errors introduced while filtering this noise. We hope to reduce these errors through improved algorithms. As the noise floor is lowered, additional effort may be needed to improve alignment and calibration stability of the hardware.

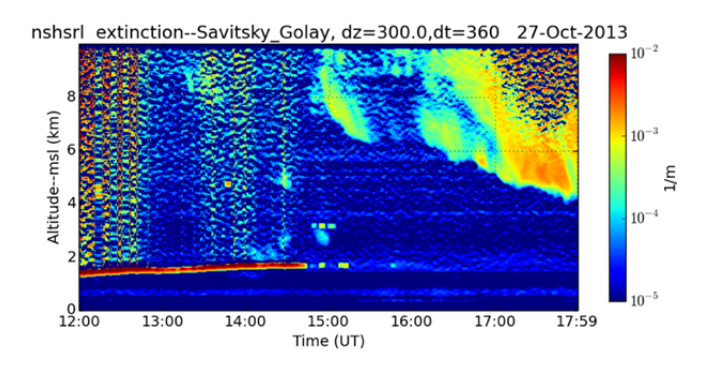


Figure 9: Extinction cross-section derived from the data used to create Figure 8. Data with molecular channel signal-to-noise ratio less than 5 are masked. Measurements where made in Barrow, Alaska.

A huge archive of HSRL data taken over many years in a wide variety of locations is available for on demand processing with user selected processing parameters at our web site [2].

# 6. Summary

Although extinction cross-section is a more useful quantity than backscatter cross-section, it is more difficult to measure. Our current hardware and algorithms provide useful measurements when the extinction is greater than ~10<sup>-4</sup> m<sup>-1</sup>. This limitation is imposed by photon counting noise and imprecise knowledge of the overlap function. We hope to improve on this noise floor by increasing the power transmitted while maintaining eye safe operation. Further improvements will be sought through improved algorithms.

# References

- [1] Eloranta, E.W., "High Spectral Resolution Lidar", in *Lidar:* Range-Resolved Optical Remote Sensing of the Atmosphere, K. Weitkamp editor, Springer-Verlag, New York, 2005.
- [2] University of Wisconsin lidar group web site: lidar.ssec.wisc.edu
- [3] Savitzky, A; Golay, M.J.E. (1964), "Smoothing and Differentiation of Data by Simplified Least Squares procedure", *Analytical Chemistry*, **36**, (8), 1627-1639.

# Biography



Ed Eloranta received a B.S. in Physics, in 1965, a M.S in Meteorology in 1967 and a PhD in Meteorology in 1972, all degrees were from the University of Wisconsin-Madison. He is a Senior Scientist at the University of Wisconsin where he has designed, constructed and

applied advanced lidars for atmospheric measurement. He is a fellow of the American Meteorological Society and a fellow of the Optical Society of America.